IEEE Photonics Journal
An IEEE Photonics Society Publication

The Input Power Dynamic Range of a Semiconductor Optical Amplifier and Its Relevance for Access Network Applications

Volume 3, Number 6, December 2011

R. Bonk, Member, IEEE
T. Vallaitis, Member, IEEE
J. Guetlein
C. Meuer
H. Schmeckebier
D. Bimberg, Fellow, IEEE
C. Koos, Member, IEEE
W. Freude, Senior Member, IEEE
J. Leuthold, Senior Member, IEEE

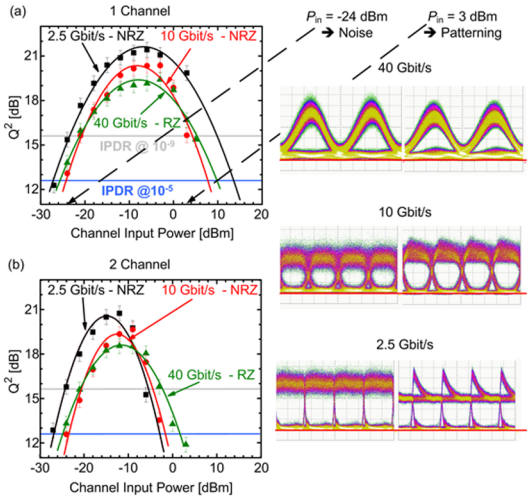

DOI: 10.1109/JPHOT.2011.2172787
1943-0655/$26.00 ©2011 IEEE

The Input Power Dynamic Range of a Semiconductor Optical Amplifier and Its Relevance for Access Network Applications

R. Bonk,[1] *Member, IEEE*, T. Vallaitis,[1] *Member, IEEE*, J. Guetlein,[1] C. Meuer,[2] H. Schmeckebier,[2] D. Bimberg,[2] *Fellow, IEEE*, C. Koos,[1,3] *Member, IEEE*, W. Freude,[1,3] *Senior Member, IEEE*, and J. Leuthold,[1,3] *Senior Member, IEEE*

[1]Institute of Photonics and Quantum Electronics (IPQ), Karlsruhe Institute of Technology (KIT), 76131 Karlsruhe, Germany
[2]Institute of Solid State Physics, Technical University Berlin, 10623 Berlin, Germany
[3]Institute of Microstructure Technology (IMT), Karlsruhe Institute of Technology (KIT), 76344 Eggenstein-Leopoldshafen, Germany

DOI: 10.1109/JPHOT.2011.2172787
1943-0655/$26.00 ©2011 IEEE

Manuscript received September 9, 2011; revised October 9, 2011; accepted October 12, 2011. Date of publication October 19, 2011; date of current version November 8, 2011. This work was supported by the Center of Functional Nanostructures (CFN) of the German Research Foundation (DFG), by the Karlsruhe School of Optics and Photonics (KSOP), by the European project EURO-FOS, by the Karlsruhe Nano-Micro Facility (KNMF), by Sonderforschungsbereich SFB 787, and by the German Federal Ministry of Education and Research (BMBF) in the project CONDOR. Corresponding author: R. Bonk and J. Leuthold (e-mail: rene.bonk@kit.edu; j.leuthold@kit.edu).

Abstract: The input power dynamic range (IPDR) of a semiconductor optical amplifier (SOA) gives the input power range within which an SOA can be operated error free. It is among the most important parameters describing the usability range of an SOA in an access network. In this paper, we give design guidelines to maximize the IPDR at a given gain. Our IPDR description indicates that a large IPDR can be obtained if SOAs are designed properly. A particular large IPDR is predicted to be found for well-designed quantum-dot (QD)-SOAs. We apply both theory and experiment to a 1.3-μm QD-SOA and investigate the IPDR as a function of bitrate, wavelength, and bias current. Large IPDRs of 41 and 36 dB are found for single-channel experiments with a signal quality of $Q^2 = 12.6$ dB at 2.5 and 40 Gbit/s, respectively.

Index Terms: Fiber optics systems, optoelectronic materials, semiconductor materials.

1. Introduction

The input power dynamic range (IPDR) is defined as the range of input powers into an amplifier at which error-free amplification of a data signal can be ensured. Semiconductor optical amplifiers (SOA) have recently found to be of highest interest for future fiber-to-the-home (FTTH) networks where they are likely to be needed to extend reach and power split ratios. In such FTTH networks, a large amplifier IPDR is of particular importance in the upstream path which carries the data from the customers to the central office (CO). Here, different clients contribute with different power levels due to their different distances to the amplifier.

FTTH deployments rapidly increase due to the requirements for high-bandwidth applications such as video-on-demand, high-definition TV (HDTV), interactive gaming, and virtual reality [1]. A possible realization for FFTH is a passive optical network (PON) [2]. Today, the Gigabit-PON (GPON) offers a physical reach of 20 km between the CO and the customer locations, a split ratio of 1:32, bitrates of up to 2.5 Gbit/s [time-division multiplexing (TDM)], and a total loss budget of 28 dB

on a single wavelength [3]. Several research activities and network vendor discussions are ongoing for extending today's access networks up to a reach of 100 km with split ratios between 256 and 1024 per wavelength [wavelength-division multiplexing (WDM)] and bitrates exceeding 1 Gbit/s per user in residential applications and exceeding 10 Gbit/s per user in business applications [4], [5]. This next-generation (NG)-PON would allow the consolidation of thousands of CO and can be implemented in a hybrid TDM/WDM approach with direct detection. For the realization of such NG-PON, a large increase of the tolerable loss is required. One option is the use of optical-electrical-optical repeaters. Alternatively, optical amplifiers can allow reach extension as well [6], [7].

Requirements on reach-extending optical amplifiers are challenging, especially in the upstream path from the customer to the CO. Here, the distance variations among customer locations may cause strong power variations at the amplifier input. This burst mode nature of the upstream data together with the probable existence of a variety of different split ratios in hybrid WDM/TDM NG-PON require amplifiers with highest IPDR. This upstream path is typically operated at 1.3 μm, at which, however, only few types of amplifiers are available.

In the past, various optical amplifier technologies have been discussed, which partly satisfied the requirement of a large IPDR. Ordinary erbium and praseodymium-doped fiber-amplifiers exhibit high gain, yet they show burst-sensitive operation and low gain bandwidth. As a result, this amplifier technology needs gain compensation techniques [6], [7]. A hybrid technology, using SOAs together with Raman amplifiers, proved to provide large bandwidths [8]. Yet, this hybrid solution still requires a Raman pump laser and offers moderate IPDR. Another promising and cost-efficient technology, which can be used as a gain element in NG-PON, is an SOA. SOAs have the potential to meet all the requirements for a NG-PON extender without gain compensation, with just a single and inexpensive chip. For example, quantum-dot (QD)-SOAs exhibit ultrafast QD gain response ($\sim$1 ps) [9], large gain bandwidth ($\sim$120 nm) [10], high gain ($>$ 25 dB), and a low noise figure ($<$ 5 dB) [11], [12]. They can be operated without cooling [13], have high burst mode tolerance [14], and introduce low chirp even under gain saturation [15]. Further, they are expected to become polarization insensitive in the future [16].

In this paper, we discuss the IPDR of such SOAs. Guidelines to design SOAs with large IPDR are given. For this purpose, an IPDR description is introduced, and the respective parameters are determined. It is shown that QD-SOAs with a low number of QD-layers (low optical confinement) and long devices provide potentially the best IPDR for a particular gain. We find an IPDR larger than 35 dB at 40 Gbit/s for gain that exceeds 15 dB at a target bit error ratio (BER) of 10^{-9}. In single- and two-channel experiments, we operate the QD-SOAs error free at bitrates of 2.5 Gbit/s, 10 Gbit/s, and 40 Gbit/s with on-off keying (OOK) modulation. We report IPDR up to 41 dB for measurements with one data channel at 2.5 Gbit/s at a BER of 10^{-5}. Even for the two-channel operation, an IPDR of 28 dB at a bitrate of 40 Gbit/s at a BER of 10^{-5} is found. IPDR dependence on wavelength and bias current is addressed.

The paper is structured as follows: Section 2 covers the description of the IPDR, Section 3 presents the SOA device properties, and Sections 4–7 show the IPDR measurement results as a function of bitrate, wavelengths, rival signal, and bias current. Finally, the measurement results from Section 7 are used to derive device design guidelines in Section 8.

2. Description of IPDR

The IPDR is defined as the SOA input power range within which error-free amplification is achieved; see Fig. 1(a). In this paper, we use the term error free for two cases. The first case requires a signal quality of $Q^2 = 15.6$ dB which corresponds to a BER of 10^{-9} in the case of a system only limited by additive white Gaussian noise. In the second case, a forward error correction (FEC) coding is used in the PON, which allows error-free operation for Q^2 of 12.6 dB corresponding to a BER of 10^{-5}. A Q^2 of 12.6 dB is better than what will be required for NG-PON where bit error ratios around 10^{-4} are tolerated together with FEC [3].

The IPDR limitation P_1^{in} on the low input power side is due to a low optical signal-to-noise ratio (OSNR), whereas the IPDR limitation P_2^{in} on the high input power side is due to gain saturation

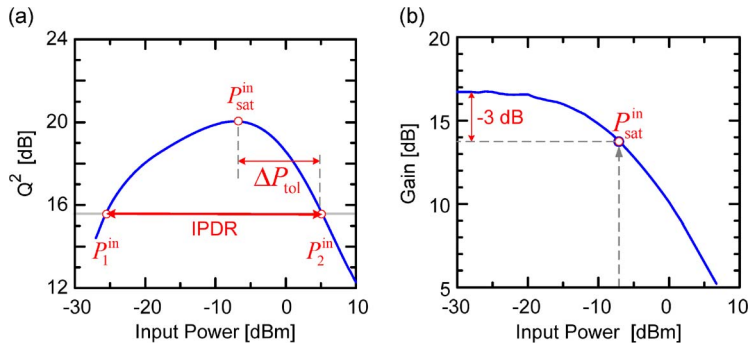

Fig. 1. Definition of the input power dynamic range (IPDR). (a) The IPDR is defined as the SOA input power range within which error-free amplification is achieved. The lower and upper limits of the IPDR are due to a low OSNR and gain saturation, respectively. The plot also visualizes the definition of the empirical tolerance factor $\Delta P_{\text{tol}} = 10\ \text{lg}\ p_{\text{tol}} = 10\ \text{lg}\ (P_2^{\text{in}}/P_{\text{sat}}^{\text{in}})$. (b) Gain as a function of input power. The 3-dB saturation input power is marked.

induced patterning and interchannel crosstalk (multichannel experiments). The IPDR is defined as $\text{IPDR} = 10\ \text{lg}\ (P_2^{\text{in}}) - 10\ \text{lg}\ (P_1^{\text{in}})$.

In the following, an IPDR description is introduced to discuss the limitations of the signal quality and to derive device design guidelines in Section 8 of this paper. It needs to be mentioned that in this section, the parameters are all chip values.

The lower limit of the IPDR P_1^{in} may be derived starting with the well-known electrical signal-to-noise ratio $\text{SNR} = Q^2$ equation for incoherent direct detection with optical amplification [17] considering a reasonable unsaturated gain $G_0 \gg 1$

$$\text{SNR} = \frac{(G_0 P^{\text{in}})^2}{4\ (G_0 P^{\text{in}})\ P_{\text{ASE}} \frac{B_e}{B_o} + 2\ P_{\text{ASE}}^2 \frac{B_e}{B_o}}. \tag{1}$$

Here, only the dominant signal-noise beating (first term in denominator) and noise-noise beating (second term in denominator) terms are considered. P_{ASE} is the amplified spontaneous emission power from the SOA, which is copolarized with the signal, P^{in} is the optical input power to the SOA, B_o the optical filter bandwidth, and B_e the electrical filter bandwidth. Resolving (1) for the lower limit of the IPDR P_1^{in} for the case of error-free amplification $\text{SNR}_{\text{min}} = Q_{\text{min}}^2$ gives

$$P_1^{\text{in}} = \left[\sqrt{2\ \text{SNR}_{\text{min}} B_e B_o + 4\ \text{SNR}_{\text{min}}^2 B_e^2} + 2\ \text{SNR}_{\text{min}} B_e\right] P_{\text{ASE}}/G_0 B_o \tag{2}$$

with

$$P_{\text{ASE}} = n_{\text{sp}}(G_0 - 1)\ hf \cdot B_o. \tag{3}$$

Here, n_{sp} is the inversion factor, h is the Planck constant, and f is the optical carrier frequency.

A strategy to minimize P_1^{in} is to decrease the amplified spontaneous emission power P_{ASE} from the SOA. For minimization of the ASE output power a perfect inversion is required, i.e., the inversion factor is $n_{\text{sp}} \rightarrow 1$. Here, the QD-SOA technology in principle should have an advantage compared with conventional bulk or QW-SOA since their carrier reservoir should be able to make a perfect inversion possible at a lower current density [18].

The upper limit of the IPDR P_2^{in} is limited by bit patterning induced by gain saturation. We derive P_2^{in} with a rate-equation SOA model neglecting nonlinearities, facet reflectivity, and ASE noise for time-independent quantities [19]. Further, a linear relation between the modal net gain g and the carrier density N is assumed. Then, we write

$$P_2^{\text{in}} = p_{\text{tol}} P_{\text{sat}}^{\text{in}}, \qquad P_{\text{sat}}^{\text{in}} = \frac{hf\ 2\ \ln(2)}{G_0 - 2} \frac{\text{A}}{\Gamma} \frac{1}{a} \frac{1}{\tau_c} \tag{4}$$

with

$$G_0 = \exp(gL) = \exp((\Gamma g_m - \alpha_L)L) = \exp(\Gamma a\ (N - N_0)\ L), \qquad N = r\tau_c. \tag{5}$$

p_{tol} describes an empirical tolerance factor of which the upper IPDR limit P_2^{in} is larger than the steady-state 3-dB saturation input power P_{sat}^{in}; see Fig. 1(b). In Fig. 1(a), the tolerance factor is expressed in logarithmic units $\Delta P_{tol} = 10 \lg p_{tol} = 10 \lg P_2^{in} - 10 \lg P_{sat}^{in}$. A is the area of the active region; Γ the optical confinement factor; a is the differential gain; g_m is the material gain; α_L expresses losses; τ_c is the effective carrier lifetime; L is the length of the device; N_0 is the carrier density at transparency; and $r = I/eV$ is the carrier generation rate with the bias current I, the active volume V, and the elementary electric charge e. It should be mentioned that the carrier density N is understood as the sum of the wetting layer carriers and the actual number of carriers in all QDs. This simplification allows us to use only one rate equation to describe all carriers in the device [20].

A strategy to maximize P_2^{in} is to increase the saturation input power P_{sat}^{in}. This in turn may be obtained by minimizing the unsaturated gain G_0, with a small effective carrier lifetime τ_c, a low differential gain a, and by a large modal cross section A/Γ.

In maximizing P_2^{in}, the QD-SOA technology offers some inherent advantages. First, the modal cross section A/Γ is large because of the low optical confinement factor Γ in QD of around 1% per layer. Second, if the reservoir states are sufficiently filled due to a large injection rate, the QD states are refilled within 1–10 ps. Thus, the QD states are highly occupied in this case, assuring a low differential gain a [18] and an ultrafast operation [9].

However, it needs to be mentioned that a well-engineered bulk or QW-SOA might have comparable performance with its QD-SOA counterpart [21]–[23].

3. SOA (1.3-μm) Device Structure and Characterization

The SOAs used in this study are grown by molecular beam epitaxy. They consist of 10 layers of InGaAs/GaAs QD with a dot-in-a-well structure [24].

The chip length is 4 mm, and the ridge waveguide width is 2 μm (sample 1) and 4 μm (sample 2), respectively. The waveguides are tilted by 8° to minimize reflections at the facets. The applied current is 490 mA for sample 1 in all measurements and varied in the measurements with sample 2. The QD-SOA provide maximum unsaturated fiber-to-fiber (FtF)-gain G_0 up to 15.5 dB (sample 1) and 17 dB (sample 2), respectively. The FtF-noise figure is around 10 dB, the 3-dB gain bandwidth is 40 nm, and the saturation output power is 10 dBm. The gain of the device is polarization dependent by up to 10 dB.

A typical FtF-gain spectrum of these devices is shown in Fig. 2(a), measured at sample 1. The gain peak is around 1295 nm. For this steady-state characterization, the temperature is set to 20 °C, and the input power is −10 dBm. Fig. 2(b) shows the linear behavior of this device for a large range of input power levels measured at the same device. The gain G is constant within a 1-dB margin for channel input powers between −30 dBm and 0 dBm for one continuous wave (cw) channel at 1310 nm and up to −6 dBm for two channels measured on 1310 nm with another cw signal launched at 1290 nm. Such a degree of linearity is only known from the linear optical amplifier approach [25], which is a specifically designed SOA using strained bulk or multiquantum well structures [22], [23], [26] and holding beam techniques in SOA [27]. Fig. 2(c) shows the amplified spontaneous emission (ASE) power spectrum of sample 2 for different bias currents measured with a resolution bandwidth of 0.1 nm. The QD ground state gain increases with current (gain peak around 1.3 μm). The maximum ground state gain is reached at a bias current of around 300 mA due to complete inversion. A further bias current increase leads to a reduction in ground state gain due to device heating. The excited state gain peak is close to 1.2 μm. The excited states are not fully inverted within the range of current measured here.

The 3-dB saturation input powers P_{sat}^{in} and the unsaturated gain G_0 of samples 1 and 2 are presented in Table 1 for two wavelengths. The bias current of sample 1 and sample 2 is 490 mA and 300 mA, respectively. The temperature is set to 20 °C. The saturation input power levels of the two samples are not comparable due to different unsaturated gains, waveguide widths, and

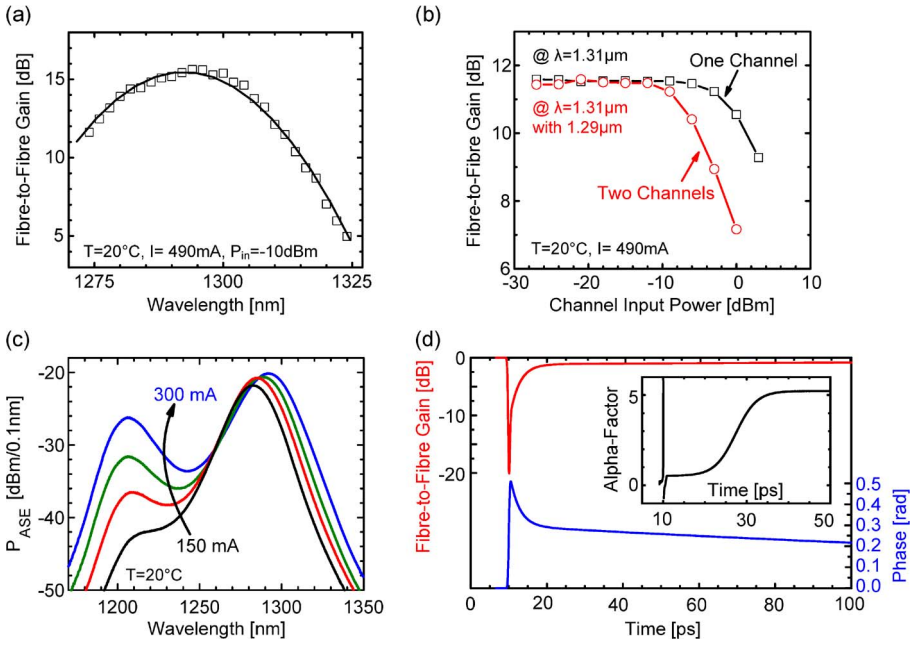

Fig. 2. Typical 1.3-μm QD-SOA characteristics of the measured devices. (a) A 3-dB gain bandwidth of 40 nm at 1.295 μm with a peak gain of 15 dB is found with sample 1. (b) Fiber-to-Fiber gain as a function of the input power, showing linear behavior over a huge range of input power levels. The gain is constant within a 1-dB margin for channel input power levels of up to 0 dBm for the single-channel case and up to -6 dBm for the two-channel case. (c) Typical QD-SOA amplified spontaneous emission (ASE) power spectrum for different bias currents at sample 2. (d) The gain and the phase response of the QD-SOA are plotted. A fast (1–10 ps) and a slow (100–200 ps) time constant are visible. The overall phase effects are weak, however, and dominated by the slow component. The inset shows a low time-dependent effective alpha-factor measured on sample 2.

TABLE 1

Saturation input power and unsaturated gain as a function of wavelength for sample 1 and sample 2. Sample 1 is operated with a bias current of 490 mA, and sample 2 is operated with 300 mA. The bias currents correspond to current densities of around 6 kA/cm^2 for sample 1 and 2 kA/cm^2 for sample 2, respectively. The temperature is set to 20°

	Wavelength 1290 nm		Wavelength 1310 nm	
	Sample 1	Sample 2	Sample 1	Sample 2
Saturation input power P_{sat}^{in}	2 dBm	-7 dBm	4 dBm	-4 dBm
Unsaturated gain G_0	15.5 dB	17 dB	11.5 dB	14 dB

supplied current densities, which are around 6 kA/cm^2 for sample 1 and around 2 kA/cm^2 for sample 2.

The dynamic behavior of the QD-SOA in a pump-probe experiment is shown in Fig. 2(d) [9]. The QD-SOA (sample 2) has a fast and a slow carrier refilling time. The fast time constant is in the order of 1–10 ps and is due to a quick refilling of the QDs by the reservoir. The slow time constant in the order of 100–200 ps is due to the refilling of the reservoir states [9]. The gain recovery is dominated by the fast time constant. Contrarily, the phase response is dominated by the slow component. The inset in Fig. 2(d) shows that the effective alpha-factor—which is defined as the ratio of phase and gain changes—is not constant (as assumed by many SOA simulation programs). It strongly changes with time under a large signal modulation [28]. From the pump-probe measurement results, we know that in a QD-SOA, fast and slow processes influence the gain and the phase dependence simultaneously but with different magnitudes: The gain depletes strongly but recovers

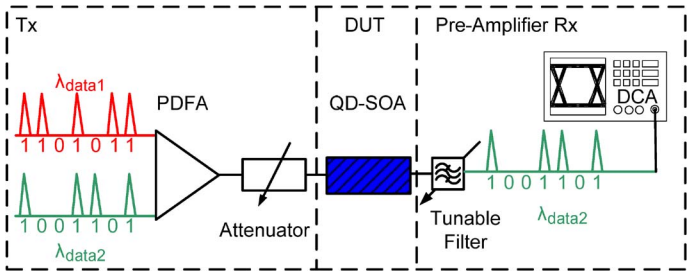

Fig. 3. Setup to measure IPDR of the SOA device under test (DUT). The quality of the OOK-data signals (Q^2-factor) after amplification in an SOA are measured for single and two channel operation at bitrates of 2.5 Gbit/s, 10 Gbit/s, and 40 Gbit/s, while the input power is varied. In the two channel operation mode, the signals are decorrelated. The quality of the received signal is measured with a pre-amplifier receiver.

fast. In contrast, the phase recovers slowly. Therefore, the effective alpha-factor changes with time. The alpha-factor of the first 10 ps after the strong pump pulse is governed by the refilling of the depleted QD states from the reservoir. This depletion can be described as a spectral-hole-burning (SHB) process with an alpha-factor close to zero. The depleted reservoir states lead to an increased alpha-factor $(t > 20$ ps$)$, which remains large until the reservoir states are slowly refilled by external carrier injection.

4. IPDR Dependence on Bitrate

The IPDR of the 1.3-μm QD-SOA is studied for single and multiple data signals at various bitrates. Experiments are performed with the setup shown in Fig. 3. Two decorrelated data signals are adjusted to various power levels before launching the composite signal into the SOA. After the SOA, one channel is blocked by a tunable filter, while the Q^2-factor of the remaining data channel is analyzed with a digital communications analyzer (DCA). The receiver is operated 10 dB above its sensitivity threshold of $Q^2 = 15.6$ dB.

We investigate the IPDR for bitrates of 2.5 Gbit/s NRZ-OOK, 10 Gbit/s NRZ-OOK, and 40 Gbit/s RZ-OOK with sample 1. First, a single data signal at a wavelength of 1310 nm is generated. Its power at the SOA input is varied, and the quality of the received signal is measured. Second, two decorrelated data signals at a wavelength of 1310 nm and 1290 nm are generated. Their power is kept at the same level and varied from -27 dBm to 5 dBm. The SOA is operated at a current of 490 mA. Its temperature is set to 20 °C.

The sensitivity of the Q^2-factor to variations in the power launched into the SOA for the single-channel case is shown in Fig. 4(a). An IPDR exceeding 25 dB is found at all bitrates for a Q^2-factor of 15.6 dB (gray line within the figure). The IPDR for a Q^2-factor of 12.6 dB is estimated to exceed 32 dB for all bitrates (light blue line within the figure).

At low launch powers, the signal performance degrades as the device is operated below the OSNR limit. The small deviations in Q^2-factor between the bitrates at low launch powers arise from electrical bandwidth adjustments for different bitrates at the DCA and the use of a precision time base at 40 Gbit/s only.

In the high input power limit, the signal quality is affected by patterning that dominates when the SOA is operated in saturation and the QD-SOA dynamic is too slow to follow the pattern [29]. At 2.5 Gbit/s, both the slow gain dynamic of the reservoir, as well as the fast QD refilling, are clearly able to follow the data streams. We therefore find error-free operation up to highest input powers. At 10 Gbit/s, where the QD-SOA is operated with a bit-period that is comparable with the slow 100-ps carrier refilling time, we observe strong overshooting; see the eye diagram in Fig. 4. At 40 Gbit/s, the influence of the slow carrier refilling leads to patterning. Since the pulses are shorter than the slow carrier refilling time, the effect statistically averages out. The patterning is therefore not too severe. Conversely, the influence of the fast QD gain dynamic on the amplification process increases. Due to the fact that the fast effect has the same time scale as the bit-period of the 40 Gbit/s data signal, it leads to a gain compression that acts almost equally onto all bits. This explains why the

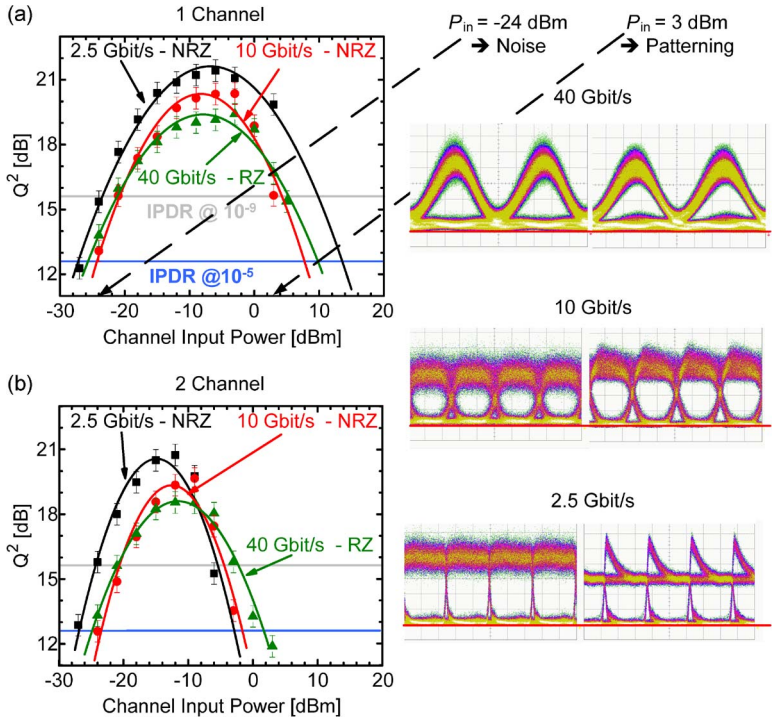

Fig. 4. Q^2-factor of one and two channels amplified with a QD-SOA versus channel input power at bitrates of 2.5, 10, and 40 Gbit/s. (a) In the single channel case we find an IPDR ($Q^2 = 12.6$ dB marked by the light blue line) between 32 dB and 41 dB for 2.5 Gbit/s, 10 Gbit/s, and 40 Gbit/s, respectively. Eye diagrams show the IPDR limitations in the single channel case. For high input powers the signal quality is limited by overshooting (2.5 Gbit/s) and patterning (10 Gbit/s and 40 Gbit/s). For low input powers the signal quality is limited by noise. (b) In the two channel case we find an IPDR ($Q^2 = 12.6$ dB) in the range of 22 dB to 27 dB for bitrates of 2.5, 10, and 40 Gbit/s. The IPDR results for a $Q^2 = 15.6$ dB are marked by the gray line.

IPDR of the 40-Gbit/s RZ data signal is comparable with the 10-Gbit/s NRZ data signal. Fig. 4 also shows the eye diagrams at the lower and upper limit of the IPDR for the different bitrates.

The results of the two channel experiments are plotted in Fig. 4(b). The IPDR becomes almost independent of the bitrate.

At low input powers, the signal qualities are similar to the single-channel case. This is to be expected since the SOA is unsaturated, and operation is only noise limited.

In the high input power limit, the SOA is operated in saturation, and we observe signal degradations due to patterning from one channel, as well as due to interchannel crosstalk [30]. The upper IPDR limit is reached when the total input power approaches the saturation input power. For our SOA with a 3-dB saturation input power of 4 dBm at a wavelength of 1310 nm (see Table 1), the upper IPDR limit therefore is close to 0 dBm for each of the two channels. This behavior may be understood by the fact that the interchannel crosstalk between two decorrelated channels may occur with a random time delay. As a consequence, the crosstalk between the channels leads to a degradation which is almost independent of the tested bitrates.

The absolute values of the IPDR measured with sample 1 at 1310 nm for the two decorrelated signals at, e.g., 10 Gbit/s are 16 dB and 22 dB at Q^2 of 15.6 dB and 12.6 dB, respectively. These values, which are measured with the QD-SOA, are comparable with the results reported for the linear optical amplifier (LOA) in [25].

5. IPDR Dependence on Wavelength

The results for the IPDR depend on the wavelength of the data signal. This is mostly due to the wavelength dependence of the unsaturated gain G_0, which influences the saturation input power;

TABLE 2

Summary of IPDR dependence on wavelength, bitrates, signal quality factor (BER), and channel number. In the single channel case, the IPDR for different bitrates is larger at wavelength with lower gain. In the two channel case, the IPDR measured at the gain peak is larger due to reduced cross-gain modulation distortions

	IPDR [dB] 1 channel measured at				IPDR [dB] 2 channels measured at			
	1290 nm		1310 nm		1290 nm		1310 nm	
Bitrate [Gbit/s]								
2.5 – NRZ OOK	36	28	41	33	28	23	24	19
10 – NRZ OOK	25	18	32	25	24	18	22	16
40 – RZ OOK	33	24	36	26	28	20	27	19
BER (Q^2 measured)	10^{-5}	10^{-9}	10^{-5}	10^{-9}	10^{-5}	10^{-9}	10^{-5}	10^{-9}

see (4). The IPDR results for measurements at wavelengths of 1290 nm and 1310 nm with sample 1 are summarized in Table 2. Measurements are performed at bitrates of 2.5 Gbit/s, 10 Gbit/s and 40 Gbit/s for the single and also for the two channel case. For the two channel experiments, the decorrelated data signals always carry the same bitrate and the same channel input power.

The spectral IPDR dependence to the most part correlates with the spectral gain dependence. The higher the gain and thus the lower the saturation input power the lower the IPDR in the single-channel case. This agrees well with (4) and is in agreement with our results in Table 2, where the IPDR at 1310 nm (11.5 dB gain, saturation input power of 4 dBm) exceeds the IPDR found at 1290 nm (15.5 dB gain, saturation input power of 2 dBm). The IPDR at 1310 nm exceeds the IPDR at 1290 nm by 5 dB at 2.5 Gbit/s, by 7 dB at 10 Gbit/s and by 2 dB at 40 Gbit/s.

In the 2 channel situation, the spectral dependence of the IPDR is affected most by the channel at the gain peak wavelength, i.e., the channel around the gain peak (1290 nm) degrades the channel measured at 1310 nm (outside of the gain peak) to larger extent than *vice versa*. More precisely, the IPDR measured at 1290 nm exceeds the IPDR at 1310 nm at all bitrates. However, the signal degradations still stem from patterning from one channel and from interchannel crosstalk. The IPDR differences between 1290 nm and 1310 nm are 4 dB at 2.5 Gbit/s, 2 dB at 10 Gbit/s, and 1 dB at 40 Gbit/s.

6. IPDR Dependence on Input Power for a Rival Signal at Gain Peak

Results of an SOA IPDR worst-case scenario, i.e., with a rival signal at the gain peak, are presented in Fig. 5 for experiments performed with sample 2. A 10-Gbit/s NRZ-OOK data signal at a wavelength of 1290 nm is launched into the QD-SOA together with a 40-Gbit/s RZ-OOK data signal at a wavelength of 1310 nm. The first serves as a rival signal on the 40-Gbit/s signal. A 10-Gbit/s signal was chosen as its bit-slot period is in the order of the slow gain dynamic of the device caused by the reservoir refilling. This represents a case with large cross-gain and cross-phase modulation distortions. The IPDR of the 40-Gbit/s signal is analyzed for three different input power levels of the rival signal. First, a low input power in the unsaturated gain regime of the SOA of -12 dBm is chosen. Then, a moderate input power of -9 dBm and, finally, an input power of -6 dBm is used which is saturating the gain of sample 2 (see Table 1). Despite the rival signal, the IPDR is large and exceeds 25 dB for a Q^2 of 15.6 dB, as long as the input power level of the rival signal is moderate (< -9 dBm). Higher input power levels of the rival signal cause maximum interchannel crosstalk, which decreases the IPDR of the 40-Gbit/s signal. Sample 2 is operated with a bias current of 300 mA at a temperature of 20 °C.

7. IPDR Dependence on Bias Current

The IPDR dependence on bias current at a given gain is investigated for a single-channel experiment with a 40-Gbit/s RZ-OOK data signal. When adapting the bias currents from 150 mA to

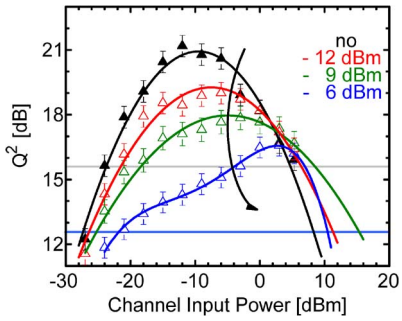

Fig. 5. IPDR dependence on input power for a rival signal at the gain peak. A 40-Gbit/s RZ-OOK data signal at a wavelength of 1310 nm is launched to the QD-SOA, together with a rival 10-Gbit/s NRZ-OOK data signal at a wavelength of 1290 nm. The IPDR of the 40-Gbit/s signal is analyzed for three different input power levels of the rival signal. The IPDR is large, as long as the input power level of the distorting signal is moderate. The gray line indicates the IPDR results for a Q^2 of 15.6 dB, whereas the light blue line indicates the IPDR results for a Q^2 of 12.6 dB.

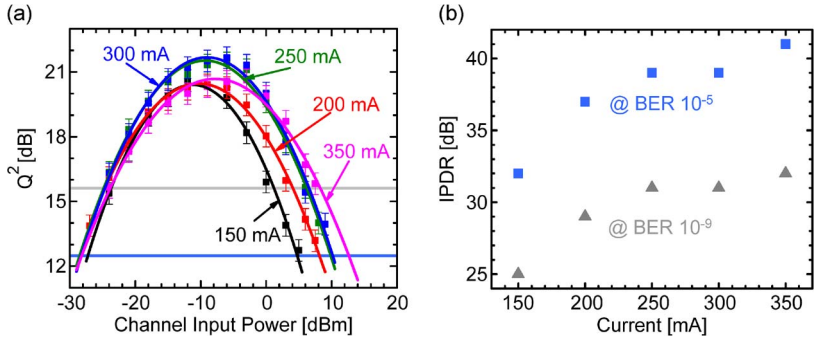

Fig. 6. IPDR dependence on bias currents for sample 2. (a) Signal quality measurement over input power for different bias currents for a 40-Gbit/s RZ-OOK signal. (b) IPDR derived from (a) as a function of the bias current. The higher the current is, the larger the IPDR. It exceeds 30 dB for a Q^2 of 15.6 dB and 40 dB for a Q^2 of 12.6 dB. Throughout the measurements, the wavelength has always been adjusted to keep a constant gain of 15 dB.

350 mA, we tune the wavelength of our test signal such that the unsaturated gain G_0 of sample 2 maintains 15 dB. This tuning is performed to eliminate effects from the gain onto the saturation power. The wavelength is thus changed from 1289.5 nm $(I = 150$ mA$)$ to 1307 nm $(I = 350$ mA$)$.

The signal quality as a function of channel input power for different bias currents is presented in Fig. 6(a). The IPDR for a Q^2 of 12.6 dB, as well as for Q^2 of 15.6 dB, is indicated. Fig. 6(b) shows the IPDR as a function of bias current for Q^2 of 12.6 dB (light blue squares), as well as for Q^2 of 15.6 dB (gray triangles). The maximum IPDR is exceeding 40 dB for a Q^2 of 12.6 dB and 30 dB for a Q^2 of 15.6 dB. In general, the IPDR improves with larger bias currents. The IPDR increases monotonously up to 41 dB for a Q^2 of 12.6 dB and up to 32 dB for a Q^2 of 15.6 dB. From Fig. 6(a), it can be seen that the lower input power limit of the IPDR hardly changes with the bias current. However, the upper IPDR limit increases monotonously with increasing bias current. We attribute this increase of the saturation input power mostly to the reduction of the effective carrier lifetime, [see (4)] since the unsaturated power gain and the modal cross section are constant, and therefore, they cannot contribute to the improvement. The effective carrier lifetime in (4) can be interpreted as the slow carrier refilling time of the reservoir states in the QD-SOA. A larger bias current causes a higher population of the reservoir states and, thus, an efficient and fast refilling of the QD states.

8. SOA Device Design Guidelines for Large IPDR With Moderate Gain

In this section, design guidelines to optimize the IPDR of an SOA are given. For this, we use the IPDR description derived in Section 2. The IPDR description is first validated with parameters

derived from our experiments presented in Sections 3 and 7. Actually, all required parameters can be derived from steady-state characterization and 40-Gbit/s OOK measurements of the IPDR at different currents and at a constant gain of 15 dB, as described in Figs. 2(c), 6(a), and 8(a).

It is shown that low QD-layer numbers and long devices provide the best IPDR for a particular gain.

8.1. Experimental Parameter Determination for IPDR Description

To use the IPDR description for P_1^{in} and P_2^{in} as derived in (2) and (4), we need measured values of the saturation input power $P_{\text{sat}}^{\text{in}}$, the unsaturated gain G_0, and the ASE output power P_{ASE}. For this, we perform steady-state and dynamic measurements on sample 2 at various currents and input powers. The IPDR description of the SOA device was derived for chip-to-chip values $(P_1^{\text{in}}, P_2^{\text{in}}, G_0)$, while in the experiment, we measure FtF values $(\text{FtF-}P_1^{\text{in}}, \text{FtF-}P_2^{\text{in}}, \text{FtF-}G_0)$. In order to adapt, measured and chip values losses of 4 dB per facet have to be accounted for. The results within this and within the following paragraphs are always displaying the FtF values.

To calculate the lower limit of the IPDR FtF-P_1^{in} according to (2), we use the values of the steady-state measurements of P_{ASE} from Fig. 2(c) at an unsaturated gain $G_0 = 15$ dB. As mentioned in Fig. 6, we tuned the wavelength to keep G_0 at a value of 15 dB. Here, the system parameters of the optical bandwidth B_{o} and the electrical bandwidth B_{e} of a 40-Gbit/s system are used; see Table 3. The calculated values for the lower IPDR limit [open triangles in Fig. 7(a)] are compared with the IPDR measurement results from Fig. 6(a) for a 40-Gbit/s signal at a Q^2 of 15.6 dB [filled triangles in Fig. 7(a)]. It can be seen that calculated and measured values agree well.

The lowest P_1^{in} is obtained when the inversion factor is smallest which is to be expected from theory, see (2) and (3). This behavior is supported by the plots shown in Fig. 7(a) and (b). Fig. 7(a) shows the P_1^{in} versus the SOA bias currents. The lowest value is found at $I = 250$ mA. Fig. 7(b) shows the calculated inversion factor. Its value is lowest at $I = 250$ mA, which was to be expected from the IPDR description. The inversion factor n_{sp} in Fig. 7(b) has been calculated with (3) using the experimental data for P_{ASE} at the gain $G_0 = 15$ dB, taking into account the respective signal wavelengths (corresponding photon energy hf) at a specific bias current. n_{sp} decreases for increasing current levels up to 250 mA. This is due to a higher population inversion of the QD states. A further current increase leads to carrier excitations from the QD ground state due to thermal issues, which causes an increase in the inversion factor.

In the following the upper limit of the IPDR P_2^{in} is discussed. Fig. 8(a) shows the FtF-gain versus the input power for different bias currents for the discussed measurement procedure. The 3-dB saturation input powers $P_{\text{sat}}^{\text{in}}$ are indicated by circles. $P_{\text{sat}}^{\text{in}}$ increases with the bias current. Next, we extract the upper limit of the IPDR P_2^{in} at different bias currents from the measured results in Fig. 6(a) and plot the saturation input power $P_{\text{sat}}^{\text{in}}$ versus the upper limit of the IPDR P_2^{in}; see Fig. 8(b). It may be seen that the QD-SOA upper IPDR limit is offset from the steady-state saturation input power by the tolerance factor ΔP_{tol} of around 12 dB.

The effective carrier lifetime τ_{c}, as well as the differential gain a, cannot easily be measured. However, the device parameters τ_{c}/N_0 and aN_0 can be derived from measurements using (4) and (5). We have plotted the results in Fig. 8(c) and (d) as a function of the bias current. It is obvious that the effective carrier lifetime (reservoir refilling time) reduces for operating points with higher bias currents due to a larger occupation of the reservoir. The differential gain only slightly changes.

Now, all parameters of the device and the system are known, which enables us to predict design guidelines for large IPDR with moderate gain. A summary of all the parameters is shown in Table 3.

8.2. Design Guidelines to Optimize SOAs for Largest IPDR With Moderate Gain

The IPDR description allows us to derive guidelines for designing SOAs with large IPDR. Important parameters that we can control are the device length L, the number of QD-layers, the confinement factor Γ, the waveguide cross section A, and the doping concentration of the active region material or the bias current.

TABLE 3

Device and system parameters used for the optimization process and a QD-SOA active region schematic

	Parameter	Value
Known Device Parameters	Confinement factor per layer	Γ = 1 %
	Waveguide width	w = 4 μm
	Waveguide height	h = 0.5 μm
	Active region height per QD layer	h′ = 40 nm
	Waveguide cross section	$A = w \cdot h$ = 2*10^{-12} m^2
Known System Parameters for 40 Gbit/s OOK	Optical bandwidth	B_O = 2 nm
	Electrical bandwidth	B_e = 50 GHz
	Electrical SNR	SNR = 36
Fixed Parameters Obtained from Parameterization in Paragraph 8.1	Generation rate	$r = I/eV$ = 2.8·10^{-32} s^{-1}m^{-3}
	Wavelength	λ = 1300 nm
	Inversion factor	n_{sp} = 1.5
	Empirical tolerance factor	ΔP_{tol} = 12 dB
	Normalized carrier lifetime	τ_C / N_0 = 5.97*10^{-33} s m^3
	Normalized differential gain	aN_0 = 1.77*10^4 m^{-1}

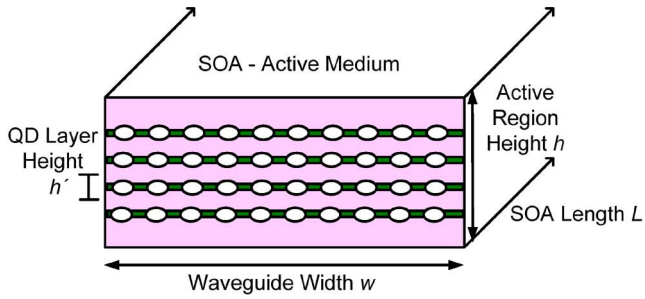

The upper limit of the IPDR P_2^{in} is given by (4) and (5). For a given unsaturated gain G_0 and a specific ΔP_{tol}, we can write

$$P_2^{in} \propto \frac{1}{G_0}\frac{A}{\Gamma}\frac{1}{\tau_c}\frac{1}{a}, \qquad G_0 = \exp\left[\Gamma a\left(\frac{I\,\tau_c}{eV} - N_0\right)L\right]. \tag{6}$$

This leads us to the following strategy to maximize P_2^{in}:

- *Choose G_0 as small as possible to serve the purpose:* From (6), we see that a minimum gain must be stipulated as the IPDR could go to infinity for smallest gain values.
- *Large modal cross section A/Γ with small confinement factor.* This is obtained by adapting the device geometry and choosing the SOA type accordingly, e. g., the confinement factor of a QW or QD-SOA is lower than the confinement factor of a bulk SOA. However, a decrease in the confinement causes a decrease in the unsaturated gain, which can be compensated by an increase in the device length and/or a higher bias current I.
- *Lifetime-doping of the active region material* [31]. A lifetime-doping can cause a reduction of the effective carrier lifetime. However, the gain is again decreased, and the already-discussed measures have to be taken.

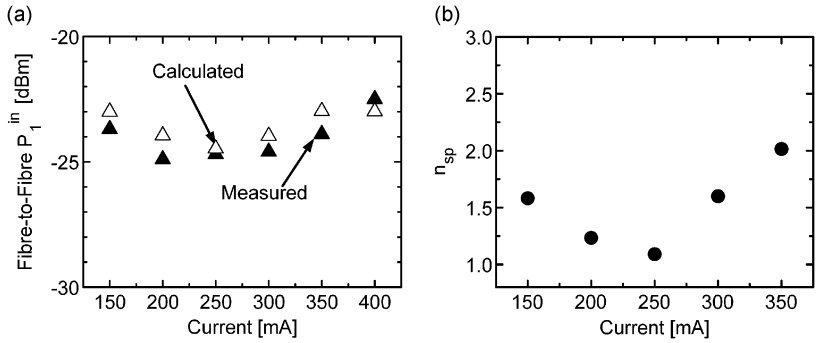

Fig. 7. Measured and calculated values of the lower limit of the IPDR for different bias currents and the inversion factor. (a) Measured values of the lower limit of the IPDR for different operating points (filled triangles) showing good agreement with the calculated values (open triangles). The calculated values are obtained applying our IPDR description to the ASE output power and the unsaturated gain from steady-state characterization. (b) The inversion factor as a function of current. The inversion factor reaches its lowest value of almost 1 at a current of 250 mA. The values are derived from the steady-state characterization of the ASE output power and the unsaturated gain.

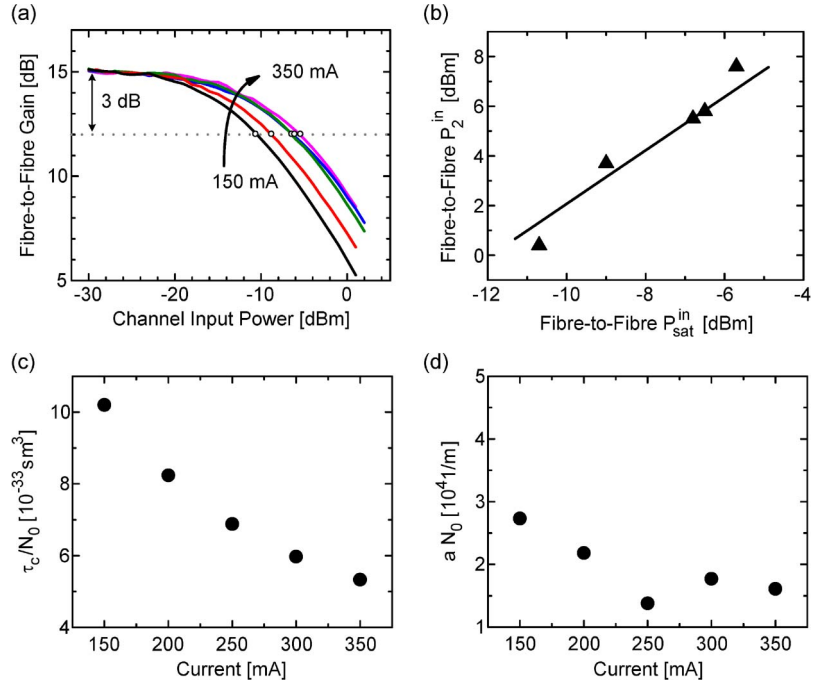

Fig. 8. Important device parameters of sample 2. (a) FtF-Gain as a function of input power for different bias currents. The 3-dB saturation input powers at various bias currents are marked by circles. They increase with the bias currents. For the plots at different currents, the wavelength of the data signal is always adjusted to guarantee a constant unsaturated gain of 15 dB. (b) P_2^{in} versus P_{sat}^{in} for different bias currents. It can be seen that P_2^{in} and P_{sat}^{in} are always offset by 12 dB. The values for P_2^{in} are derived from Fig. 6(a) and that the values for P_{sat}^{in} are obtained from (a). (c) The effective carrier lifetime per carrier density at transparency for different current values as derived from the unsaturated gain and the saturation input power. A higher carrier density due to higher current reduces the effective carrier lifetime. (d) Differential gain times the carrier density at transparency for different current values derived as in (c). The lowest differential gain is achieved at a current of 250 mA.

- *High bias current I*. The increase in bias current causes a reduction in the effective carrier lifetime. Then, the unsaturated gain increases. It can be compensated by reducing the SOA length or the confinement. It needs to be mentioned that the unsaturated gain cannot be increased arbitrarily. Thermal effects might decrease the inversion.

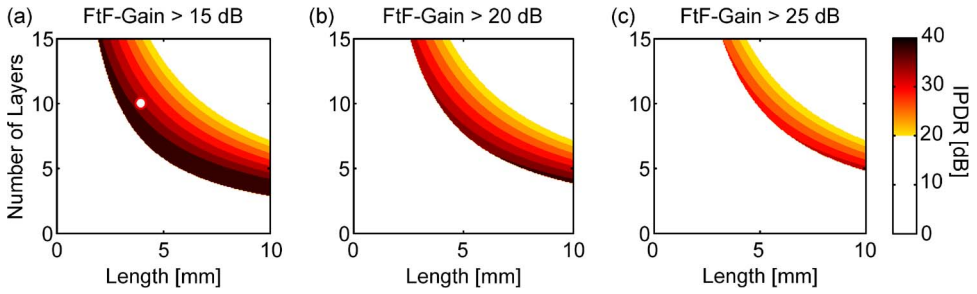

Fig. 9. Region for device parameters where the fiber-to-fiber gain and the IPDR are larger than defined minimum values. For required values of the gain, a low number of QD-layers and long waveguides provide the best IPDR. The circle indicates the IPDR result measured with sample 2 at 300 mA.

- *Low differential gain a.* In theory *a* is expected to increase if the dimensionality of the electronic system of the active medium is reduced. This is, i.e., in QD active regions, due to the delta-function like density of states, which should lead to quite a strong change in the gain, even for small carrier density variations. However, in practice the differential gain of QD-SOAs are not as large because the size of QDs varies significantly, and the QD energy states are thus spread across a larger spectral range. The decrease in gain due to the decrease in the differential gain can again be counteracted by a device length increase or a larger bias current.

The lower limit of the IPDR P_1^{in} is given by (2) and (3). From these equations, we derive that for a given unsaturated gain $G_0 \gg 1$, the lower limit of the IPDR P_1^{in} is proportional to the inversion factor: $P_1^{\text{in}} \propto n_{sp}$. The population inversion can be optimized by adapting the current accordingly, i.e., choosing it as high as possible. This will minimize the lower IPDR limit.

Subsequently, we use the IPDR description to exemplarily derive design guidelines for a QD-SOA with a FtF-gain of 15–25 dB and an IPDR of 25–40 dB. In general, we perform the study for different device lengths as well as for differing QD-layer numbers. From the discussion above, we expect that longer devices with a lower confinement factor are preferable. All simulations are performed at 1.3 μm with a constant carrier generation rate $r = I/eV$. This way, the effective carrier lifetime and the differential gain are constant. The current is always adapted because a variation of the QD-layer number and device length changes the active volume $V = \text{QD layer number} \cdot h' \cdot w \cdot L$ (h' is the active region height per QD-layer, and w is the waveguide width). The confinement is assumed to be 1% per layer [18].

First, the unsaturated gain G_0 is calculated with (5) using the experimentally determined parameters τ_c/N_0, aN_0, and r, which are presented in Table 3. Once the unsaturated gain G_0 is known, the saturation input power $P_{\text{sat}}^{\text{in}}$ can be calculated and subsequently using ΔP_{tol} the upper limit of the IPDR P_2^{in}. Since the device is operated with a constant generation rate r, the inversion factor n_{sp} may also be assumed to be constant, which enables us to calculate the ASE output power P_{ASE} with (3). Then, the lower IPDR limit FtF-P_1^{in} is calculated using (2). All parameters of the IPDR description are summarized in Table 3. The IPDR has been calculated for various gain values as a function of device length and number of QD layers. Fig. 9 shows the areas for which a particular minimal FtF-gain (a) > 15 dB, (b) > 20 dB, (c) > 25 dB, and minimal IPDR (color-coded from 0–40 dB) have been achieved. It can be seen that it is not possible to optimize device parameters in order to maximize gain and IPDR simultaneously. In general, long devices with few QD-layers combine high gain and maximum IPDR. The IPDR results measured with sample 2 at 300 mA are indicated by the circle in Fig. 9(a). Finally, it should be mentioned that in addition to varying the number of QD layers and cavity length, ridge width can also be a powerful parameter to optimize the device in terms of saturation power [19], [21], [32].

9. Conclusion

The IPDR of SOAs has been discussed in general. A description relating device parameters with the IPDR is given. The model predicts large IPDRs for SOAs with a large modal cross section, a low

confinement factor, and a long, doped active region. These parameters are favorable, especially for the upper IPDR limit, by providing a large saturation power. Further, a high bias current is preferable for a large IPDR. This is because a higher current provides a higher population inversion and, thus, less ASE noise, and it keeps the effective carrier lifetime low, which helps to further increase the saturation power. Finally, to keep IPDRs large, the gain has to be chosen just to meet the need of the application. An overly large gain degrades the IPDR significantly.

These optimum specifications for a large IPDR favor QD-SOAs over other SOA types. This is because the number of QD-layers can be chosen to be small, and a minimum gain can be maintained by choosing a long active region. Consequently, we have validated our IPDR description with QD-SOAs at 1.3 μm. In experiments, we found a large IPDR exceeding 32 dB with Q^2 values of 12.6 dB for signals at bitrates of 2.5 Gbit/s, 10 Gbit/s, and 40 Gbit/s in single-channel operation. Even for operation with multiple signals, we still found an IPDR in the range of 22 dB.

Finally, it should be emphasized that bulk, QW, and QD-SOAs that come close to or match the above derived design guidelines may as well be suitable to fulfill the requirements of NG-PONs that require reach extender with IPDR $>$ 35 dB and gain $>$ 15 dB at a target BER of 10^{-9}.

References

[1] L. G. Kazovsky, W.-T. Shaw, D. Gutierrez, N. Cheng, and S.-W. Wong, "Next-generation optical access networks," *J. Lightw. Technol.*, vol. 25, no. 11, pp. 3428–3442, Nov. 2007.

[2] E. Trojer, S. Dahlfort, D. Hood, and H. Mickelsson, "Current and next-generation PONs: A technical overview of present and future PON technology," *Ericsson Rev.*, vol. 2, pp. 64–69, 2008.

[3] Gigabit-capable Passive Optical Networks (GPON): Physical Media Dependent (PMD) Layer Specification, ITU-T Recommendation G.984.2, 03/2003, 2003.

[4] R. Davey, J. Kani, F. Bourgart, and K. McCammon, "Options for future optical access networks," *IEEE Commun. Mag.*, vol. 44, no. 10, pp. 50–56, Oct. 2006.

[5] R. P. Davey, D. B. Grossman, M. Rasztovits-Wiech, D. B. Payne, D. Nesset, A. E. Kelly, S. Appathurai, and S.-H. Yang, "Long-reach passive optical networks," *J. Lightw. Technol.*, vol. 27, no. 3, pp. 273–291, Feb. 2009.

[6] K.-I. Suzuki, Y. Fukada, D. Nesset, and R. Davey, "Amplified gigabit PON systems," *J. Opt. Netw.*, vol. 6, no. 5, pp. 422–433, May 2007.

[7] L. H. Spiekman, J. M. Wiesenfeld, A. H. Gnauck, L. D. Garrett, G. N. van den Hoven, T. van Dongen, M. J. H. Sander-Jochem, and J. J. M. Binsma, "8 $\times$ 10 Gb/s DWDM transmission over 240 km of standard fiber using a cascade of semiconductor optical amplifiers," *IEEE Photon. Technol. Lett.*, vol. 12, no. 8, pp. 1082–1084, Aug. 2000.

[8] P. P. Iannone, K. C. Reichmann, C. Brinton, J. Nakagawa, T. Cusick, E. M. Kimber, C. Doerr, L. L. Buhl, M. Capuzzo, E. Y. Chen, L. Gomez, J. Johnson, A. M. Kanan, J. Lentz, Y. F. Chang, B. Pálsdóttir, T. Tokle, and L. Spiekman, "Bi-directionally amplifier extended reach 40 Gb/s CWDM-TDM PON with burst-mode upstream transmission," presented at the Opt. Fiber Commun. Conf., Los Angeles, CA, Mar.6–10, 2011, Paper PDPD6.

[9] T. Vallaitis, C. Koos, R. Bonk, W. Freude, M. Laemmlin, C. Meuer, D. Bimberg, and J. Leuthold, "Slow and fast dynamics of gain and phase in a quantum dot semiconductor optical amplifier," *Opt. Express*, vol. 16, no. 1, pp. 170–178, Jan. 2008.

[10] R. Brenot, F. Lelarge, O. Legouezigou, F. Pommereau, F. Poingt, L. Legouezigou, E. Derouin, O. Drisse, B. Rousseau, F. Martin, and G.H. Duan, "Quantum dots semiconductor optical amplifier with a$-$3 dB bandwidth of up to 120 nm in semi-cooled operation," presented at the Opt. Fiber Commun. Conf., San Diego, CA, Feb. 24–28, 2008, Paper OTuC1.

[11] T. Akiyama, M. Sugawara, and Y. Arakawa, "Quantum-dot semiconductor optical amplifiers," *Proc. IEEE*, vol. 95, no. 9, pp. 1757–1766, Sep. 2007.

[12] D. Bimberg, "Quantum dot based nanophotonics and nanoelectronics," *Electron. Lett.*, vol. 44, no. 3, pp. 168–171, Jan. 2008.

[13] H. Wang, E. T. Aw, M. Xia, M. G. Thompson, R. V. Penty, I. H. White, and A. R. Kovsh, "Temperature independent optical amplification in uncooled quantum dot optical amplifiers," presented at the Opt. Fiber Commun. Conf., San Diego, CA, Feb. 24–28, 2008, Paper OTuC2.

[14] R. Bonk, C. Meuer, T. Vallaitis, S. Sygletos, P. Vorreau, S. Ben-Ezra, S. Tsadka, A. R. Kovsh, I. L. Krestnikov, M. Laemmlin, D. Bimberg, W. Freude, and J. Leuthold, "Single and multiple channel operation dynamics of linear quantum-dot semiconductor optical amplifier," presented at the IEEE Eur. Conf. Opt. Commun., Brussels, Belgium, Sep. 21–25, 2008, Paper Th.1.C.2.

[15] R. Brenot, M. D. Manzanedo, J.-G. Provost, O. Legouezigou, F. Pommereau, F. Poingt, L. Legouezigou, E. Derouin, O. Drisse, B. Rousseau, F. Martin, F. Lelarge, and G. H. Duan, "Chirp reduction in quantum dot-like semiconductor optical amplifiers," presented at the IEEE Eur. Conf. Opt. Commun., Berlin, Germany, Sep. 16–20, 2007, Paper We08.6.6.

[16] N. Yasuoka, K. Kawaguchi, H. Ebe, T. Akiyama, M. Ekawa, K. Morito, M. Sugawara, and Y. Arakawa, "Quantum-dot semiconductor optical amplifiers with polarization-independent gains in 1.5-μm wavelength bands," *IEEE Photon. Technol. Lett.*, vol. 20, no. 23, pp. 1908–1910, Dec. 2008.

[17] N. A. Olsson, "Lightwave systems with optical amplifiers," *J. Lightw. Technol.*, vol. 7, no. 7, pp. 1071–1082, Jul. 1989.

[18] M. Sugawara, H. Ebe, N. Hatori, M. Ishida, Y. Arakawa, T. Akiyama, K. Otsubo, and N. Nakata, "Theory of optical signal amplification and processing by quantum-dot semiconductor optical amplifiers," *Phys. Rev. B, Condens. Matter*, vol. 69, no. 23, p. 235 332, Jun. 2004.
[19] M. J. Connelly, *Semiconductor Optical Amplifiers*. Boston, MA: Kluwer, 2002.
[20] A. V. Uskov, E. P. O'Reilly, M. Laemmlin, N. N. Ledentsov, and D. Bimberg, "On gain saturation in quantum dot semiconductor optical amplifiers," *Opt. Commun.*, vol. 248, no. 1–3, pp. 211–219, Apr. 2005.
[21] K. Morito, "High-power semiconductor optical amplifier," presented at the Opt. Fiber Commun. Conf., San Diego, CA, Mar. 22–26, 2009, Paper OWQ4.
[22] C. Michie, A. E. Kelly, J. McGenough, I. Armstrong, I. Andonovic, and C. Tombling, "Polarization-insensitive SOAs using strained bulk active regions," *J. Lightw. Technol.*, vol. 24, no. 11, pp. 3920–3927, Nov. 2006.
[23] A. E. Kelly, C. Michie, I. Armstrong, I. Andonovic, C. Tombling, J. McGenough, and B. C. Thomsen, "High-performance semiconductor optical amplifier modules at 1300 nm," *IEEE Photon. Technol. Lett.*, vol. 18, no. 24, pp. 2674–2676, Dec. 2006.
[24] A. R. Kovsh, N. A. Maleev, A. E. Zhukov, S. S. Mikhrin, A. P. Vasil'ev, E. A. Semenova, Y. M. Shernyakov, M. V. Maximov, D. A. Livshits, V. M. Ustinov, N. N. Ledentsov, D. Bimberg, and Z. I. Alferov, "InAs/InGaAs/GaAs quantum dot lasers of 1.3 μm range with enhanced optical gain," *J. Cryst. Growth*, vol. 251, no. 1–4, pp. 729–736, Apr. 2003.
[25] D. A. Francis, S. P. DiJaili, and J. D. Walker, "A single-chip linear optical amplifier," presented at the Opt. Fiber Commun. Conf., Anaheim, CA, Mar. 17–22, 2001, Postdeadline Paper PDP 13-1.
[26] S. Tanaka, S.-H. Jeong, S. Yamazaki, A. Uetake, S. Tomabechi, M. Ekawa, and K. Morito, "Monolithically integrated 8:1 SOA gate switch with large extinction ratio and wide input power dynamic range," *IEEE J. Quantum Electron.*, vol. 45, no. 9, pp. 1155–1162, Sep. 2009.
[27] R. J. Manning, A. D. Ellis, A. J. Poustie, and K. J. Blow, "Semiconductor laser amplifiers for ultrafast all-optical signal processing," *J. Opt. Soc. Amer. B, Opt. Phys.*, vol. 14, no. 11, pp. 3204–3216, Nov. 1997.
[28] J. Wang, A. Maitra, C. G. Poulton, W. Freude, and J. Leuthold, "Temporal dynamics of the alpha factor in semiconductor optical amplifiers," *J. Lightw. Technol.*, vol. 25, no. 3, pp. 891–900, Mar. 2007.
[29] C. Meuer, J. Kim, M. Laemmlin, S. Liebich, A. Capua, G. Eisenstein, A. R. Kovsh, S. S. Mikhrin, I. L. Krestnikov, and D. Bimberg, "Static gain saturation in quantum dot semiconductor optical amplifiers," *Opt. Express*, vol. 16, no. 11, pp. 8269–8279, May 2008.
[30] R. Alizon, D. Hadass, V. Mikhelashvili, G. Eisenstein, R. Schwertberger, A. Somers, J. P. Reithmaier, A. Forchel, M. Calligaro, S. Bansropun, and M. Krakowski, "Cross-saturation dynamics in InAs/InP quantum dash optical amplifiers operating at 1550 nm," *Electron. Lett.*, vol. 41, no. 5, pp. 266–268, Mar. 2005.
[31] A. Kapoor, E. K. Sharma, W. Freude, and J. Leuthold, "Investigation of the saturation characteristics of InGaAsP-InP bulk SOA," *Proc. SPIE*, vol. 7597, p. 75971I, 2010.
[32] Z. Y. Zhang, R. A. Hogg, X. Q. Lv, and Z. G. Wang, "Self-assembled quantum-dot superluminescent light-emitting diodes," *Adv. Opt. Photon.*, vol. 2, no. 2, pp. 201–228, Jun. 2010.